https://doi.org/10.33263/Materials24.471476

ISSN: 2668-5728 https://materials.international

Materials International

Volume 2, Issue 4, Pages 0471-0476
2020

Received: 19.06.2020
Accepted: 2.10.2020
Published: 10.10.2020

Article

Facile Synthesis of Nano Mg-Co Ferrites (x=0.15, 0.20, 0.25, 0.30, 0.35, and 0.40) via Co-precipitation Route: Structural Characterization

Rakesh Vishwarup [1], Shridhar N. Mathad [2,*]

[1] Department of Physics. Jain P.U.College, Davanagere, Karnataka, India
[2] Department of Engineering Physics, K.L.E Institute of technology, Hubballi, 580027, Karnataka, India
* Correspondence: physiccssiddu@gmail.com; Scopus ID: 55143736400

Abstract: Cobalt doped $MgFe_2O_4$ (x=0.15, 0.20, 0.25, 0.30, 0.35, and 0.40) ferrites samples were prepared by facile synthesis route co-precipitation method. Formation of spinal cubic ferrite was confirmed by using X-ray diffraction with lattice parameters of the samples ranging from 8.207A^0 - 8.357A^0, and the crystallite size is in the range 180 A^0 - 360 A^0. The surface morphology from SEM analysis observed grain sizes in the range 4µm - 6 µm. A comparative contemplate was carried out with the help of W-H analysis and SSP analysis. An absorption band of the FTIR spectrum is employed to supports the formation of spinal cubic structure. Dislocation density, hopping lengths, and microstrain of the sample were also reported. A detailed structural study of ferrites has been reported with respect to cobalt doping.

Keywords: XRD; Co-precipitation; Ferrites; Micro strain; Dislocation density.

1. Introduction

Ferromagnetic nanomaterials are of increasing importance because of their wide applications in electric and magnetic fields [1,2]. Because of their high permeability, high electrical resistivity, low electric and magnetic losses, they are widely used in microwave devices [3]. Ferromagnetic properties of the material depending on the particle or grain size. When the particle size is large compared to the single domain size, then the material act as a hard magnet. If the particle size smaller than the single domain size, the material act as a soft magnet [4]. Ferrites are magnetic materials which exhibit ferri-magnetism. Ferrites are similar to antiferromagnets except for the fact that ferrites show spontaneous magnetization in the absence of field due to unequal dipole arrangement in the opposite direction [5,6]. Ferrite contains iron oxide as its principal component, with one or more metal cations [7]. The chemical formula of ferrite is MFe_2O_4 (M = divalent metal ion, e.g., Mn, Mg, Zn, Ni, Co, Cu, etc.). Ferrites can be doped with more number of metal ions, their chemical formula changes by adding another metal ion [8]. Where divalent metal ion and trivalent metal ion, which will occupy tetrahedral and octahedral sites, respectively in normal spinel ferrite [9]. Magnesium ferrite is an inverse spinel

Cite This Article: Vishwarup, R.; Mathad, S.N.Facile synthesis of Nano Mg-Co ferrites(x=0.15, 0.20, 0.25, 0.30, 0.35, and 0.40)via coprecipitaion route: structural characterization. Mat Int **2020**, 2, 0471-0476. https://doi.org/10.33263/Materials24.471476

ferrite where maximum trivalent ions occupy tetrahedral sites, and remaining trivalent and divalent ions occupy octahedral sites [10]. Soft ferrites have unique properties such as high curie temperature, high saturation magnetization, and low coercivity. So, they are widely used in microwave absorbers and high-frequency electronic instruments. Cobalt ferrite is also inverse spinel ferrite, but it is known as hard ferrite compared to magnesium ferrite because of high coercivity [11]. On doping with cobalt, the coercivity of Mg ferrite increases. And also, lesser ionic radii of cobalt causes shrinkage of a unit cell of Mg-ferrite [12].

Ferrites can be synthesized by many techniques such as solid-state reactions [13], co-precipitation technique [14], sol-gel combustion [15], modified oxidation process [16], forced hydrolysis [17], hydrothermal process [18], ball-milling [19], Pulsed laser deposition [20], Sputtering [21] and aerosol method [22]. In which the co-precipitation method is an eco-friendly, cost-effective method, which is the most frequently used method for the synthesis of ferrites.

In this manuscript we established the structural properties of $Mg_{1-x}Co_xFe_2O_4$ (x=0.15, 0.20, 0.25, 0.30, 0.35, and 0.40) nanoparticles synthesized by co-precipitation method. The structural properties of ferrites have been explored by XRD, SEM, and FTIR studies. We have Compared the unit cell volume, X-ray density, microstrain, and crystallite size of samples with different concentrations of cobalt doping, also correlated these results with W-H and SSP plots. The surface morphology of samples with different concentrations of cobalt is done, and grain sizes were compared and reported.

2. Materials and Methods

2.1. Synthesis.

All samples were synthesized by the co-precipitation method [22]. Analytical grade compounds of $MgCl_2.4H_2O$, $CoCl_2.2H_2O$, and $FeCl_3.6H_2O$ were dissolved separately in distilled water (150CC each) to produce an ionic solution. Ammonia solution is added dropwise until we get a pH of 8. During this process, metal hydroxides were formed, further formation of $Mg_{1-x}Co_xFe_2O_4$ ferrites. The precipitate is powdered by using mortar and crusher. The well-powdered sample is heated to 550^0 C for 6 hours by using a Muffle furnace. The schematic diagram representing the synthesis process is shown in Fig.1.

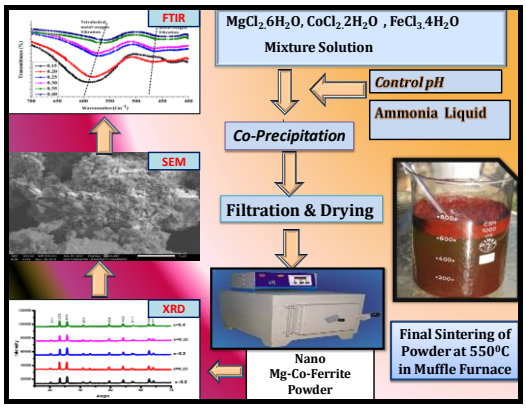

Figure 1. The schematic diagram for the synthesis of ferrites.

3. Results and Discussion

3.1 XRD analysis.

The XRD patterns of $Mg_{1-x}Co_xFe_2O_4$ ferrites are given in fig2 with the peaks(1 1 1), (2 2 0), (3 1 1), (4 0 0), (3 3 1), (4 2 2),(5 1 1), (4 4 0) and (5 3 1) confirms the cubic spinal structure which is confirmed with the help of (JCPDC card #00-084-0542) of $MgFe_2O_4$[32,33].The detailed information such as lattice parameter, unit cell volume, crystallite size, X-ray density, bond lengths, dislocation density and microstrain are given in the table1 for different concentrations (that is for x=0.15, 0.2, 0.25, 0.3, 0.35 and 0.4) are calculated using the following equations[23] and presented in Table 2.

The Crystallite size *(D)* calculated by using the Debye–Scherer equation is

$$D = 0.9\lambda / \beta \cos\theta \quad (1)$$

The Dislocation density and micro strain are calculated by using equations

$$\rho_D = \frac{1}{D^2} \quad (2)$$

$$\varepsilon = \beta \cos\theta / 4 \quad (3)$$

$$\rho_D = \frac{15\varepsilon}{aD} \quad (4)$$

The X-ray density (Δ_x) was calculated by the formula

$$\Delta_x = \frac{8M}{Na^3} \quad (5)$$

The Hopping length in site A (tetrahedral) and site B (octahedral) were calculated by

$$L_A = \frac{a \times \sqrt{3}}{4} \text{ and } L_B = \frac{a \times \sqrt{2}}{4} \quad (6)$$

The interatomic distances – tetrahedral bond length ($r_{A\text{-}O}$), octahedral bond length ($r_{B\text{-}O}$) calculated using

$$r_A = (u - 1/4)a\sqrt{3} - r(O^{2-}) \quad \ldots\ldots\ldots\ldots (7)$$

$$r_B = (5/8 - u)a - r(O^{2-}) \quad \ldots\ldots\ldots\ldots (8)$$

The Lattice strain η and average crystalline size D were calculated using the Williamson–Hall equation

$$\frac{\beta cos\theta}{\lambda} = \frac{1}{D} + \frac{\eta sin\theta}{\lambda} \quad (9)$$

The "size-strain plot" (SSP) is the best tool to empathize the isotropic nature and micro-strain by

$$(d_{hkl}\beta_{hkl}\cos\theta)^2 = \frac{K\lambda}{D} d_{hkl}^2 \beta_{hkl}\cos\theta) + (\frac{\xi}{2})^2 \quad (10)$$

The W-H plot and SSP analysis graphs were shown in Fig.3 and Fig.4 for the ferrite samples, respectively. Also, we have correlated these values with the calculations from the size strain plot (SSP) and Williamson-Hall (W-H) plot [24], which are given in Table2.

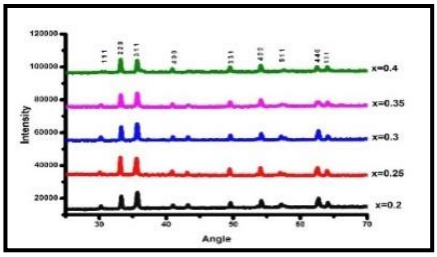

Figure 2. XRD pattern of $Mg_{1-x}Co_xFe_2O_4$ ferrite.

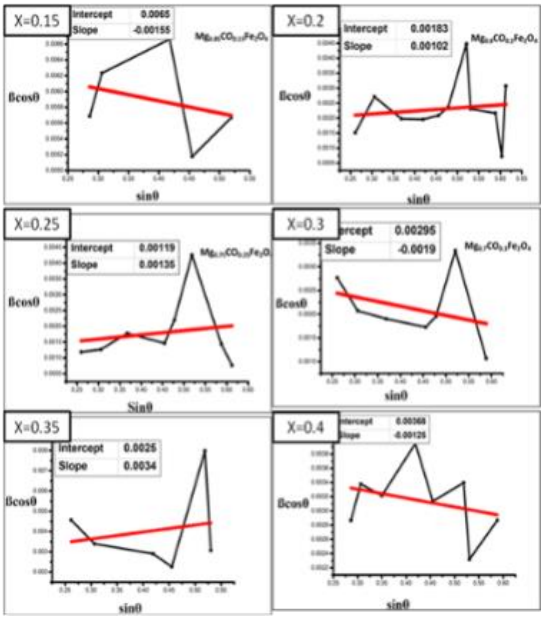

Figure 3. Williamson-Hall plots for $Mg_{1-x}Co_xFe_2O_4$ ferrites.

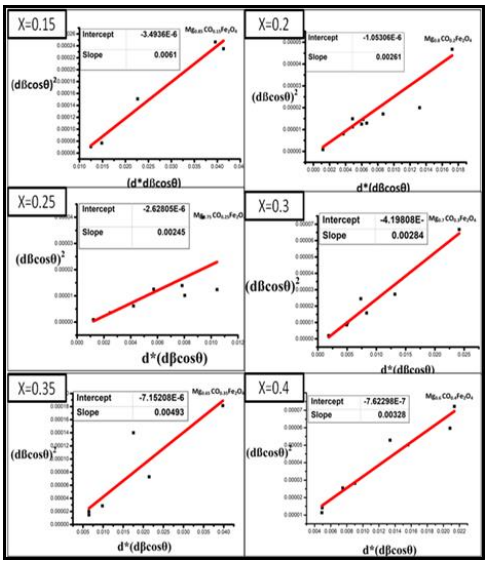

Figure 4. Size Strain Plots for $Mg_{1-x}Co_xFe_2O_4$ferrites.

3.2. SEM analysis.

The Morphological and Microstructural analysis of $Mg_{1-x}Co_xFe_2O_4$ ferrites(x=0.15, 0.2, 0.25, 0.3, 0.35 and 0.4) were carried out by using JEOL Model JSM - 6390LV.

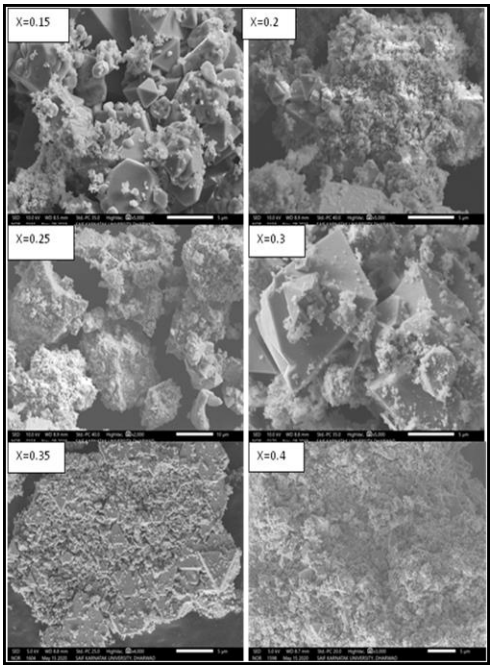

Figure 5. SEM images of the $Mg_{1-x}Co_xFe_2O_4$ series (x=0.15, 0.2, 0.25, 0.3, 0.35 and 0.4).

From the Fig.5 SEM images reveal that morphology changes continuously by varying the concentration of cobalt content. SEM images show the formation of polygon-shaped grains with a size ranging from 4.7µm - 5.4 µm. For higher cobalt

concentration, the grain size decreases because of smaller ionic radii of magnesium compared to that of cobalt. Figure 5 shows the grown nanoparticles with a relatively larger size compared to the size obtained from XRD analysis. This is because of the formation of secondary particles due to the agglomeration of primary particles with an increase of cobalt content [25].

3.3. FTIR analysis.

Fig. 6 shows FTIR spectrum of $Mg_{1-x}Co_xFe_2O_4$ (x=0.15, 0.2, 0.25, 0.3, 0.35 and 0.4) within wavelength range 400-4000 cm^{-1}. Ferrites are possessing two major bands ν_1 and ν_2, for tetrahedral metal-oxygen vibration and octahedral vibration, respectively [26, 27]. The lower absorption band is found to be between 419 cm^{-1} to 425 cm^{-1} of metal-oxygen vibration at the octahedral site. And higher absorption band is found to be between 560 cm^{-1} to 591 cm^{-1} at tetrahedral sites, as shown in Table 4. The values of ν_1 are greater than those of ν_2; it is indicating that the normal vibration mode of the tetrahedral vibration is higher than that of the corresponding octahedral sites. This may be due to a shorter bond length in the tetrahedral site [A] compared to that in the octahedral one [B]. The observed shift in band positions slightly towards lower value for ν_1 and ν_2 with increasing cobalt content [28].

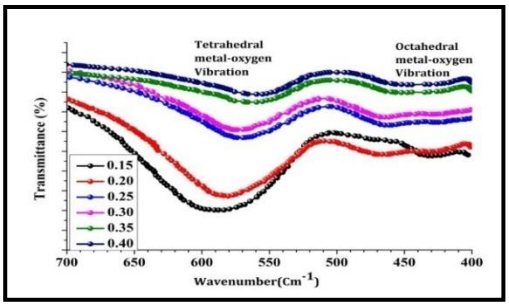

Figure 6. FTIR Spectrum of $Mg_{1-x}Co_xFe_2O_4$ ferrite.

Table 1. Lattice parameter (a), Volume of the unit cell (V), the crystallite size (D), X-ray density (d_x), Dislocation Density (ϱ_D), microstrain (ε), Hopping length L_A and L_B of $Mg_{1-x}Co_xFe_2O_4$.

X	0.15	0.2	0.25	0.3	0.35	0.4
Lattice parameter a (Å)	8.20	8.33	8.35	8.34	8.32	8.30
Volume of unit cell V (10^{-30})	567	579	583	580	577.80	571.78
Crystallite size (Å)	237.4	728	965.8	732.1	404.87	451.01
X ray density d_x gm/cm^3	4.80	4.82	4.77	4.79	4.80	4.84
Dislocation Density ϱ_D(m^{-2}) X10^{14}	17.75	1.88	1.07	1.87	6.1	4.92
MicroStrain ε X10^{-4}	14.72	5.77	4.48	5.3	10.07	7.85
Hopping length L_A (Å)	3.58	3.61	3.62	3.61	3.60	3.59
Hopping length L_B(Å)	2.93	2.95	2.95	2.95	2.94	2.93

Table 2. Comparative values of crystallite size (D), microstrain (ε), and Dislocation Density (ϱ_D) calculated by W-H plots and Size-Strain plots for $Mg_{1-x}Co_xFe_2O_4$.series

	Crystallite size (A^0)			Micro strain (ε) (X10^{-4})			Dislocation density (σ) (X10^{14})	
X	**W-H graph**	**From Eqn1**	**SSP Graph**	**WH**	**From Eqn 3**	**SSP Graph**	**$1/D^2$**	**15ε/aD**
0.15	237	237	189	15.5	14.72	37.3	27.8	11.9
0.2	841	728	442	10.2	5.77	20.5	5.10	2.18
0.25	1400	966	471	13	4.48	32.4	4.49	1.66
0.3	770	732	406	19.5	5.3	40.9	6.06	4.55
0.35	594	405	234	34.5	10.07	53.4	18.2	10.4
0.4	418	451	352	12.5	7.85	17.4	8.05	5.40

Table 3. Absorption bands and grain size for $Mg_{1-x}Co_xFe_2O_4$ ferrites.

	From FTIR		From SEM
X	**ν_1(cm^{-1})**	**ν_2(cm^{-1})**	**Average Grain Size (μm)**
0.15	591	425	4.67
0.2	583	422	4.71
0.25	570	420	5.08
0.3	569	419	5.35
0.35	566	421	4.03
0.4	560	419	3.55

4. Conclusions

$Mg_{1-x}Co_xFe_2O_4$ (x=0.15, 0.2, 0.25, 0.3, 0.35 and 0.4) ferrites were successfully synthesized and characterized. All samples have a single-phase cubic spinel structure, which is confirmed by XRD analysis and FTIR. On substitution of cobalt content, the lattice constant, unit cell volume, X-ray density crystallite size decreases due to shrinkage of the unit cell on increasing the concentration of cobalt content. Because the ionic radius of cobalt is smaller compared to ionic radius of Mg, SEM images show regular polygon structured grains with grain size 4μm – 6μm. On substitution of cobalt the grain texture turns to polyhedral with lesser microstructure homogeneity, and a variation in grains size is observed, which gradually increases with an increase in cobalt. The FTIR spectra also confirm the formation of the spinel structure, which shows two absorption bands associated with the presence of two sublattices at sites A and B.

Funding

This research received no external funding.

Acknowledgments

This research has no acknowledgment.

Conflicts of Interest

The authors declare no conflict of interest.

References

1. Hench, L.L.; West, J.K. *Principles of Electronic Ceramics*. John Wiley & Sons,**1990**.
2. Islam, S.; Sharma, P. Synthesis and Characterization of Nickel Ferrite: Role of Sintering Temperature on Structural Parameters. *Journal of Nano- and Electronic Physics* **2014**, *6*.
3. Yattinahalli, S.S.; Kapatkar, S.B.; Ayachit, N.H.; Mathad, S.N. Synthesis and structural characterization of nanosized nickel ferrite. *International Journal of Self-Propagating High-Temperature Synthesis* **2013**, *22*, 147-150,https://doi.org/10.3103/S1061386213030114.
4. Shanmugavel, T.; Raj, S.G.; Rajarajan, G.; Kumar, G.R. Tailoring the Structural and Magnetic Properties and of Nickel Ferrite by Auto Combustion Method. *Procedia Materials Science* **2014**, *6*, 1725-1730, https://doi.org/10.1016/j.mspro.2014.07.158.
5. Kulkarni, A.B; Mathad, S. N;Effect of Sintering Temperature on Structural Properties of Cd doped Co-Zn Ferrite. *Journal of Nano- and Electronic Physics* **2018**, *10*, 01001-01001, https://doi.org/10.21272/jnep.10(1).01001.
6. Vishwaroop, R.; Mathad, S.N. Synthesis, Structural, W-H plot and Size-Strain analysis of Nano cobalt doped $MgFe_2O_4$ Ferrite. *Science of Sintering,* **2019**.
7. Heck, C. *Magnetic Materials and Their Applications. Butterworths*. London, **1974**.
8. Goldman, A. *Modern Ferrite Technology*. Springer, Pittsburgh, **2006.**
9. Praveena, K.; Radhika, B.; Srinath, S. Dielectric and Magnetic Properties of $NiFe_{2-x}Bi_xO_4$ Nanoparticles at Microwave Frequencies Prepared via co-precipitation Method. *Procedia Engineering* **2014**, *76*, 1-7, https://doi.org/10.1016/j.proeng.2013.09.244.
10. Balavijayalakshmi, T.; Sudha, K.; Karthika. Investigation on structural and magnetic properties of cobalt doped magnesium ferrite nano particles.*International Journal of Chem. Tech. Research,* **2014-2015***7*,12791283,https://doi.org/10.1016/j.jart.2017.03.010.
11. Priya, A.S.; Geetha, D.; Kavitha, N.J.V. Effect of Al substitution on the structural, electric and impedance behavior of cobalt ferrite. **2019**, *160*, 453-460.

Mane, D.R.; Birajdar, D.D.; Patil, S.; Shirsath, S.E.; Kadam, R.H. Redistribution of cations and enhancement in magnetic properties of sol–gel synthesized $Cu_{0.7-x}Co_xZn_{0.3}Fe_2O_4$ ($0 \leq x \leq 0.5$). *Journal of Sol-Gel Science and Technology* **2011**, *58*, 70-79, https://doi.org/10.1007/S10971-010-2357-8.

12. Chen, D.H.; He, X.R. Synthesis of nickel ferrite nanoparticles by sol-gel method. *Materials Research Bulletin* **2001**, *36*, 1369-1377,https://doi.org/10.1016/S0025-5408(01)00620-1.

13. Parmar, V.; Modi, K.B.; Joshi, H. X-ray, SEM, far IR characterization and bulk magnetic properties of Zn 2+ substituted copper ferrite synthesized by co-precipitation technique. **1999**, *37,* 207–214.

14. Chavan, P.; Naik, L.J.I.J.E.S.R. Influence of Ni2+ ions on structural, electrical and magnetic properties of magnesium ferrospinels for humidity sensor applications. **2016**, *6*, 29-42.

15. Singhal, S.; Singh, J.;Barthwal, S.K.; Chandra, K. Preparation and characterization of nanosizenickelsubstituted cobalt ferrites (CoNiFeO). *J. Solid State Chem.* **2005**, *178*, 3183–3189.

16. Sousa, M.; Tourinho, F.A.; Depeyrot, J.; da Silva, G.; Lara, M.C.F.L. New electric double-layered magnetic fluids based on copper, nickel, and zinc ferrite nanostructures. *Journal of Physical Chemistry B* **2001**, *105*, 1168-1175.

17. Yattinahalli, S.S.; Kapatkar, S.B.; Ayachit, N.H.; Mathad, S.N. Synthesis and structural characterization of nanosized nickel ferrite. *International Journal of Self-Propagating High-Temperature Synthesis* **2013**, *22*, 147-150, https://doi.org/10.3103/S1061386213030114.

18. Hanh, N.; Quy, O.K.; Thuy, N.P.; Tung, L.D.; Spinu, L. Synthesis of cobalt ferrite nanocrystallites by the forced hydrolysis method and investigation of their magnetic properties. *Physica B: Condensed Matter* **2003**, *327*, 382-384,https://doi.org/10.1016/S0921-4526(02)01750-7.

19. Masoudpanah, S.M.; Seyyed Ebrahimi, S.A.; Ong, C.K. Magnetic properties of strontium hexaferrite films prepared by pulsed laser deposition. *Journal of Magnetism and Magnetic Materials* **2012**, *324*, 2654-2658, https://doi.org/10.1016/j.jmmm.2012.03.040

20. Guo, D.; Fan, X.; Chai, G.; Jiang, C.; Li, X.; Xue, D. Structural and magnetic properties of NiZn ferrite films with high saturation magnetization deposited by magnetron sputtering. *Applied Surface Science* **2010**, *256*, 2319-2322, https://doi.org/10.1016/j.apsusc.2009.10.059.

21. Rendale, M.K.; Mathad, S.N.; Puri, V. Thick films of magnesium zinc ferrite with lithium substitution: Structural characteristics. *International Journal of Self-Propagating High-Temperature Synthesis* **2015**, *24*, 78-82,https://doi.org/10.3103/S1061386215020053.

22. Yazdani, F.; Edrissi, M. Effect of pressure on the size of magnetite nanoparticles in the co-precipitation synthesis. *Materials Science and Engineering: B* **2010**, *171*, 86-89, https://doi.org/10.1016/j.mseb.2010.03.077.

23. Prabhu, Y.; Rao, K.; Kumar, V.; Kumari, B. X-Ray Analysis by Williamson-Hall and Size-Strain Plot Methods of ZnO Nanoparticles with Fuel Variation. *World Journal of Nano Science and Engineering* **2014**, *04*, 21-28, 21–28,https://doi.org/10.4236/wjnse.2014.41004.

24. Sajjad, M.; Ullah, I.; Khan, M.I.; Khan, J.; Khan, M.Y.; Qureshi, M.T. Structural and optical properties of pure and copper doped zinc oxide nanoparticles. *Results in Physics* **2018**, *9*, 1301-1309, https://doi.org/10.1016/j.rinp.2018.04.010.

25. Bannur, M.S.; Maddani, K.I.; Mathad, S.N.; Patil, P.S. Structural and Optical Properties of (110) Plane Textured SnO2:Zn Thin Films. *International Journal of Self-Propagating High-Temperature Synthesis* **2019**, *28*, 34-38, https://doi.org/10.3103/S1061386219010035.

26. Galagali, S.L.; Patil, R.A.; Adaki, R.B.; Hiremath, C.S.; Mathad, S.N.; Pujar, R.B. Fourier transform infrared spectroscopy and elastic properties of $Mg_{1-x}Cd_xFe_2O_4$ ferrite systems. *Songklanakarin Journal of Science and Technology* **2019**, *41*, https://doi.org/10.14456/sjst-psu.2019.125.

27. Pujar, A.S.; Kulkarni, A.B.; Mathad, S.N.; Hiremath, C.S.; Rendale, M.K.; Patil, M.R.; Pujar, R.B. Structural, Electrical, and IR Properties of $Cu_xCo_{1-x}Fe_2O_4$ (x = 0, 0.4, 1.0) Prepared by Solid-State Method. *International Journal of Self-Propagating High-Temperature Synthesis* **2018**, *27*, 174-179, https://doi.org/10.3103/S1061386218030081.